Momentum-Resolved Observation of Thermal and Quantum Depletion in a Bose Gas

R. Chang, Q. Bouton, H. Cayla, C. Qu, Alain Aspect, C. i. Westbrook, D. Clément

Momentum-resolved observation of quantum depletion in an interacting Bose gas

R. Chang,[1] Q. Bouton,[1] H. Cayla,[1] C. Qu,[2] A. Aspect,[1] C. I. Westbrook,[1] and D. Clément[1,*]

[1] *Laboratoire Charles Fabry, Institut d'Optique, CNRS, Univ. Paris Sud, 2 Avenue Augustin Fresnel 91127 PALAISEAU cedex, France*

[2] *INO-CNR BEC Center and Dipartimento di Fisica, Universita di Trento, 38123 Povo, Italy*

We report on the observation of quantum depletion in ultracold metastable Helium gases. We measure the distribution of momenta $\hbar k$ in a time-of-flight experiment with single atom sensitivity. With a dynamic range spanning five decades in density, we observe dilute, high-momentum tails decaying as k^{-4}, as predicted by Bogoliubov theory. We investigate the momentum distribution for various temperatures and clearly separate and identify the quantum and thermal contributions to the depletion of the condensate. Finally we show that the population in the k^{-4}-tails associated to the quantum depletion increases with the in-trap condensate density.

In quantum systems, intriguing many-body phenomena emerge from the interplay between quantum fluctuations and interactions. Quantum depletion is an emblematic example of such a quantum many-body effect, occurring in one of the simplest many-body systems: a gas of interacting bosons at zero temperature. In the absence of interactions, the ground state consists of all particles occupying the same single-particle ground state. Taking into account inter-particle repulsive interactions at the mean-field level leads to a similar solution where all particles are condensed in the same one-particle state, whose shape is determined by the trapping potential and the interactions. In a beyond mean-field approach, which can be interpreted as taking into account quantum fluctuations and two-body interactions, the description is dramatically different. The many-body ground state consists of several components: a macroscopically occupied single-particle state, the condensate, and a population of single-particle states different from the condensate.

This description applies to diverse bosonic systems such as superfluid Helium [1], exciton-polaritons [2] and degenerate Bose gases [3]; it has also found analogies in phenomena such as Hawking radiation from a black-hole [4] and spontaneous parametric down conversion in optics [5]. The fraction of atoms not in the condensate at zero temperature, the quantum depletion, increases with the strength of inter-particle interactions and with the density, rising up to 90% in liquid ^{4}He [1]. In ultracold gases, where the density is significantly smaller, the quantum depletion usually represents a small fraction (less than 1%) of the total population. At non-zero temperature there is an additional contribution to the population of single-particle states above the condensate, originating from the presence of thermal fluctuations. So far, evidence of the quantum depletion phenomenon has been obtained through measurements of the total depleted fraction [1, 6, 7]. Here we investigate the microscopic signatures of the condensate depletion predicted by the Bogoliubov theory and observe momentum distributions associated with both the quantum depletion and the thermal excitations.

For weakly interacting systems, Bogoliubov theory describes quantum and thermal contributions to the condensate depletion [8, 9]. This approach shows that the elementary, low-energy excitations are collective quasi-particle (phonon) modes, as has been verified in experimental studies with liquid ^{4}He [10], degenerate quantum gases [11] and exciton-polaritons [2]. At zero temperature, the many-body ground state is defined as a vacuum of these quasi-particle modes. When projected on to a basis of single-particle states with momentum $\hbar k$, the many-body ground state exhibits a distribution $n(k)$, which scales as k^{-4} at large k. These power law tails do not exist in the mean-field descriptions, in which the momentum distribution has a finite extent. At non zero temperature, the contribution to $n(k)$ induced by thermal fluctuations decays exponentially for energies larger than the temperature. These various contributions are difficult to distinguish in real space, where they overlap. In contrast, they can be clearly identified in momentum space, as we show in this work.

In this letter, we report on the observation of the momentum-space signatures of quantum depletion in a gas of interacting bosons. We investigate the atomic distribution after a long time-of-flight, for various temperatures. We find that the gas is made of three components that can be unambiguously identified: the condensate (**I**), the thermal cloud (**II**) and the quantum depletion (**III**). In particular we observe the k^{-4} power-law scaling of the momentum atomic density associated with the quantum depletion. In addition, the amplitude of the k^{-4}-tails increases with the atom number and condensate density as expected.

Our experiment is performed with a Bose-Einstein condensate (BEC) of metastable Helium-4 atoms (^{4}He*). Cigar-shaped condensates, of typically $N = 2\times10^5$ ^{4}He* atoms in the 2^3S_1 state are produced in an optical dipole trap with trapping frequencies $\omega/2\pi = (438, 419, 89)$ Hz [12, 13]. After abruptly turning off the optical trap, we detect the gas with a micro-channel plate (MCP) [14, 15], after a 55 cm free-fall corresponding to a time-of-flight (TOF) of $\sim$ 330 ms. Because of the 20 eV internal energy of ^{4}He*, the MCP allows us to detect atoms individually and to record the two-dimensional (2D) position

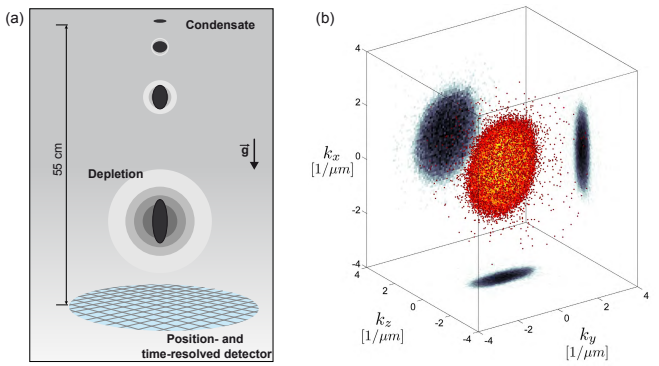

FIG. 1. **(a)** Sketch of cloud expansion and detection by a micro-channel plate detector, yielding the 3D asymptotic momentum distribution (far-field regime). The initially cigar-shaped Helium condensate (black) undergoes anisotropic expansion, inverting its aspect ratio. Quantum depletion and/or thermally excited atoms (grays) populate momentum states beyond those associated with the condensate, and are expected to have a spherical symmetry. **(b)** Measured 3D distribution of atoms $n_\infty(\mathbf{k})$ after a 330 ms time-of-flight. The central dense part corresponds to the condensate while the isolated dots are excited particles outside of the condensate wavefunction. Also shown are the 2D projections, highlighting the condensate anisotropy.

and the arrival time of each atom in the plane of the detector. The arrival time of each atom directly yields the vertical coordinate, so that we reconstruct the complete 3D atom number distribution, in contrast with usual optical imaging which yields a 2D column-integrated density. Another advantage of micro-channel plates operated in counting mode is their extremely low dark count rate. Here it allows us to investigate the atomic density over more than 5 decades (see below).

The detector is placed 55 cm below the trapped atom cloud (see Fig. 1(a)), so that after switching off the trap, the observation is made in the far-field regime where finite-size effects of the source can be safely neglected. In the free-falling frame of reference, we thus identify the position $\mathbf{r}$ of a detected atom (with respect to the cloud center) with a momentum component $\mathbf{k} = m\mathbf{r}/\hbar\bar{t}$, where $\bar{t} = 330$ ms is the time-of-flight of the cloud center [16]. It yields the asymptotic momentum distribution $n_\infty(\mathbf{k})$ obtained from the density distribution of the expanding cloud $n(\mathbf{r}, \bar{t})$, according to the ballistic relationship

$$n_\infty(\mathbf{k}) = (\hbar\bar{t}/m)^3 \; n(\mathbf{r}, \bar{t}) \qquad (1)$$

The distribution $n_\infty(\mathbf{k})$ should not be confused with the in-trap momentum distribution $n(\mathbf{k})$, since the initial phase of the expansion is affected by the interactions between the atoms. Nevertheless, as we argue below, the high-momentum tails of $n_\infty(\mathbf{k})$ provide interesting information on the momentum distribution $n(\mathbf{k})$ of the trapped atoms.

An example of $n_\infty(\mathbf{k})$ is shown in Fig. 1(b). The main component is the pancake-shaped distribution expected for the cigar-shaped condensate according to the mean-field description of the expansion [17, 18]. We also distinguish momentum components beyond those of the condensate, with a much lower density and an isotropic distribution [16]. From 3D distributions $n_\infty(\mathbf{k})$, we obtain radial and longitudinal profiles as shown in Fig. 2 [16]. With our detector we can detect high momentum components at ultra-low density. The resulting profiles exhibit several distinct features which can be grouped into three regions, as illustrated in Fig. 2(b).

Firstly, the observed distributions are dominated by the high-density condensate (region **I**: $k \equiv |\mathbf{k}| < 1.7\ \mu m^{-1}$). The initial expansion of the condensate is driven by inter-particle interactions, resulting in an asymptotic distribution different from the in-trap momentum distribution. These dynamics is fully captured by a mean-field theory, and exhibit two features. On the one hand, the size and shape of the density is well described by the scaling solution calculated in the Thomas-Fermi approximation [17, 18], as shown in Fig. 2(b). On the other hand, the mean-field Gross-Pitaevskii solution beyond the Thomas-Fermi approximation leads to the appearance of additional momentum components in the asymptotic distribution. A complete mean-field calculation for a pure condensate with our experimental parameters shows that this second effect is negligible [16].

Beyond the anisotropic condensate we observe high-momentum tails ($k > 1.7\ \mu m^{-1}$) with spherical symmetry: we attribute these components (regions **II** and **III** in Fig. 2(b)) to the condensate depletion, as discussed now. The *isotropic* character of the atomic distribution in the tails indicates that the *anisotropic* mean-field potential describing the interactions in the condensate does not play a significant role in the expansion of particles belonging to regions **II** and **III**. Thus we assume in the following that the high-momentum components of the tails, which quickly escape the condensate, are not affected by the mean-field potential during the expansion. The tails are visible over three decades in density, allowing us to perform a detailed study of their variation with momentum. We observe two distinct regimes: a middle region without a well-defined power-law variation (region **II**: $1.7 < k < 4.3\ \mu m^{-1}$), and a high-momentum region with density varying as k^{-4} (region **III**: $k > 4.3\ \mu m^{-1}$).

A quantitative description of the condensate depletion close to zero temperature is provided by Bogoliubov's microscopic theory, which yields a beyond mean-field description taking into account quantum and thermal excitations [8, 9]. In the Hamiltonian with interactions this approach retains only quadratic terms in the particle operators a_k, where a_k is the operator annihilating a particle with momentum $\hbar k$. The simplified Hamiltonian can be diagonalized by introducing the quasi-particles operators b_k according to the Bogoliubov transformation $b_k = u_k a_k + v_{-k} a^\dagger_{-k}$ [8, 9]. The occupation number of

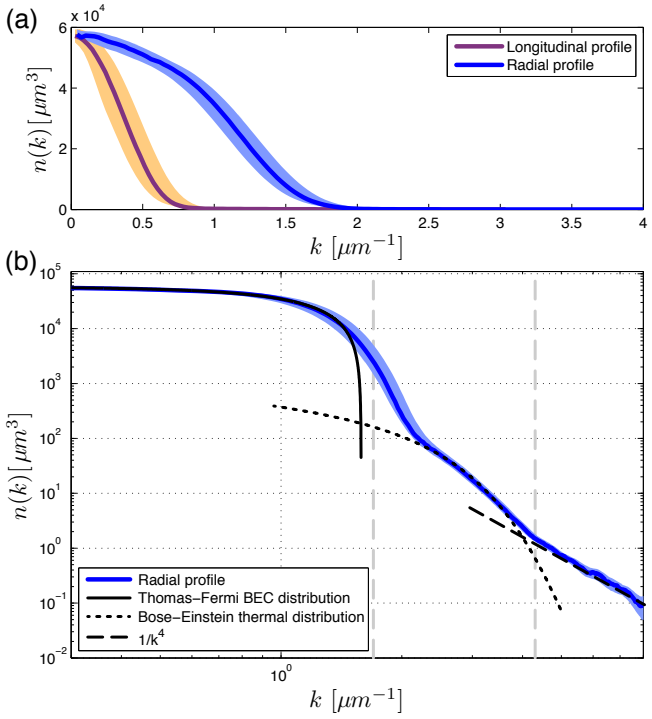

FIG. 2. 1D momentum profiles obtained from cuts of the 3D data $n_\infty(\mathbf{k})$. **(a)** Profiles along the radial (blue) and longitudinal (purple) directions. In linear scale, the tails are not visible **(b)** Log-log scale plot of the radial profile. The solid line is the scaling solution for the condensate in the Thomas-Fermi approximation (region **I**: $k < 1.7\ \mu m^{-1}$); the dash-dotted line is a Bose distribution fitting the thermal wings (region **II**: $1.7 < k < 4.3\ \mu m^{-1}$); the dashed line is a k^{-4} power-law fitting the high-momentum tails (region **III**: $k > 4.3\ \mu m^{-1}$). Solid lines are a smoothed average of the density data, and the lightly shaded band is the running standard deviation.

the non-interacting quasi-particles is given by a Bose-Einstein distribution,

$$\langle b_k^\dagger b_k\rangle = \frac{1}{\exp(\epsilon(k)/k_BT) - 1} \qquad (2)$$

where $\epsilon(k)$ is the Bogoliubov dispersion relation, k_B is Boltzmann's constant and T is the thermodynamic temperature.

The particle occupation number of non-zero momentum k can be expressed analytically in terms of the quasi-particle occupation number:

$$n(k) = \langle a_k^\dagger a_k\rangle = (|u_k|^2 + |v_k|^2)\langle b_k^\dagger b_k\rangle + |v_k|^2. \qquad (3)$$

The interpretation of the two contributions in Eq. 3 is illuminating. The first term, proportional to $\langle b_k^\dagger b_k\rangle$, represents the population of quasi-particles induced by the finite temperature. At zero temperature, this term is null and one is left with the second contribution only, $|v_k|^2$, the quantum depletion of the Bose condensate. It has no classical analog, and can be seen as arising from an interplay of Bose statistics and interactions.

According to this description, the particle occupation number $n(k)$ associated with the quantum depletion varies inversely with the momentum k for $k\xi \ll 1$ ($|v_k|^2 \propto 1/k$), and as k^{-4} for $k\xi \gg 1$, where ξ is the healing length of the condensate. The small k behavior is intimately related to the Heisenberg inequality associated with the particle and the density operators [19]. The large k behavior arises due to the two-body contact interaction and defines Tan's contact constant, a universal quantity that connects contact interactions to the thermodynamics of a many-body system [20, 21]. On the other hand, the depletion associated with the thermal excitations varies differently with k due to the additional term $\langle b_k^\dagger b_k\rangle$. In particular, the finite temperature contribution decays exponentially for $k\lambda_{dB} \gg 1$, where $\lambda_{dB} = \sqrt{h^2/2mk_BT}$ is the de Broglie wavelength. These differences provide a means to unambiguously distinguish the quantum depletion from the thermal depletion.

The presence of a trap does not modify the prediction for the condensate depletion at momenta large compared to the inverse system size $1/R \simeq 0.08\ \mu m^{-1}$, where the Bogoliubov theory in the local density approximation (LDA) is valid. For a harmonically trapped gas, a LDA calculation reproduces the large-momentum scaling k^{-4} of the homogeneous model allowing us to associate the measured k^{-4}-tails with the quantum depletion [16]. On the other hand, the thermal depletion distribution in a trap approaches a polylog function at high temperature [3]. This form is a good fit to the experimental data for $k\xi \gg 1$, as illustrated in Fig. 2(b).

To confirm our identification of the components in regions **II** and **III**, we have investigated the momentum distribution as a function of temperature. Fig. 3 presents the radial distributions $k^4 \times n_\infty(k)$ for clouds submitted to a controlled heating sequence [16]. As the cloud is heated, the distributions show an increase of the wings we associate with the thermal component, exhibiting no power-law scaling and fitting well to a polylog function. We extract an apparent temperature T_a from the polylog fit [22]. As the temperature is increased, the thermal population grows and expands over larger momenta. Beyond the thermal component, the k^{-4} tails remains visible and can be identified with the quantum depletion. Such a k^{-4} scaling has been previously reported in strongly interacting Fermi gases [23, 24]. With bosons it has been indirectly probed through radio-frequency spectroscopy [25] but it has remained elusive in momentum-space investigations [26]. In contrast to these experiments, which were conducted on short time scales close to Feshbach resonances, our studies are carried out in the weakly interacting regime, for which condensate lifetimes are on the order of seconds.

The quantum depletion is predicted to increase with the scattering length a_s and the condensate density, a variation which is captured by the Tan contact constant $\mathcal{C}$ at large momenta ($k \gg \xi^{-1}$) where $n(k) \simeq \mathcal{C}/k^4$.

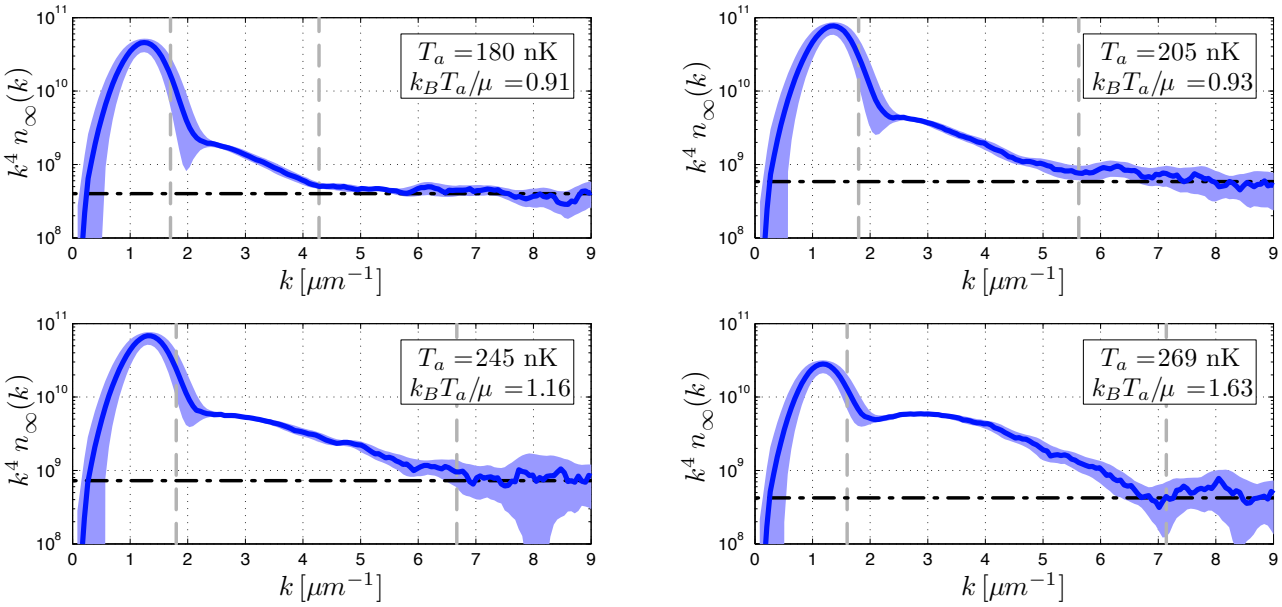

FIG. 3. Measured $k^4 n_\infty(k)$ plotted as a function of k and at various low temperatures. Vertical dashed lines delimit the momentum regions associated with the condensate, the thermal tails, and the quantum depletion. The horizontal dashed line is a fit from which the asymptotic contact constants $\mathcal{C}_\infty = \lim_{k\to\infty} k^4 n_\infty(k)$ are extracted in each subplot. Noted for each curve are the temperature T_a (see text) and the ratio of the thermal energy and the condensate energy, k_BT_a/μ.

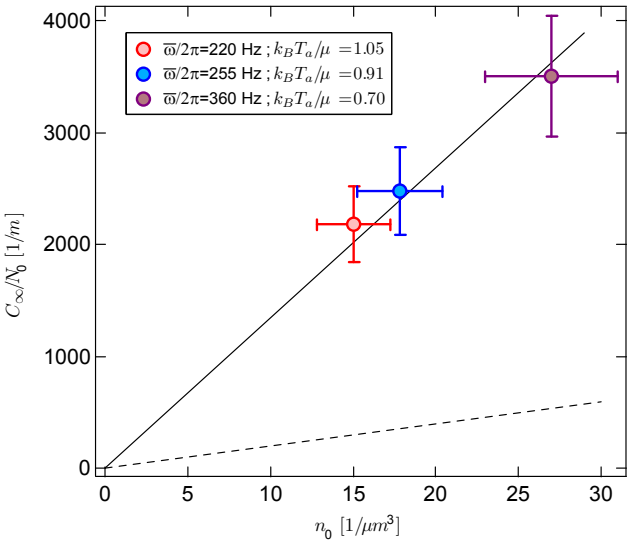

FIG. 4. Contact constant $\mathcal{C}_\infty/N_0$ per condensed particle plotted as a function of the condensate density n_0. For each measurement, the geometric trapping frequency $\bar{\omega}/2\pi$ and the ratio k_BT_a/μ are indicated. The dashed line is the Bogoliubov prediction in the LDA (see text). The solid line is the Bogoliubov prediction multiplied by a factor 6.5.

In the Bogoliubov description $\mathcal{C}$ varies as $\mathcal{C} \propto a_s^2 N_0 n_0$, with N_0 the condensate atom number and n_0 the condensate density at the center [20, 21, 25]. In the experiment, we extract a contact constant $\mathcal{C}_\infty$, defined as $\mathcal{C}_\infty = \lim_{k\to\infty} k^4 n_\infty(k)$, for various condensate densities n_0. The results are plotted in Fig. 4. We find that the contact constant $\mathcal{C}_\infty/N_0$ per condensed particle is indeed proportional to the condensate density n_0, further confirming our interpretation. The measured values $\mathcal{C}_\infty$ are about 6 times larger than the prediction of the Bogoliubov theory in the LDA approximation [16]. A quantitative understanding of this discrepancy is beyond the scope of the present work as a complete description of the many-body expansion remains a theoretical challenge.

In conclusion we have observed the microscopic signatures associated to the many-body phenomenon of quantum depletion in an interacting Bose gas. The probe we use is well suited to investigate the scaling of atomic densities with momentum, allowing us here to distinguish the contributions of quantum and thermal fluctuations to the depletion of the condensate. The single-atom detection method of metastable Helium gases is also able to provide signals of atom-atom correlations in momentum, a feature we intend to use in the future to explore momentum-space signatures of many-body effects.

We acknowledge fruitful discussions with L. P. Pitaevskii, S. Stringari and all the members of the Atom Optics group at LCF. We thank F. Nogrette for providing technical support on the MCP detector and M. Mancini for a careful reading of the manuscript. We acknowledge financial support from the Région Ile-de-France (DIM Daisy), the RTRA Triangle de la Physique, the European Research Council (Senior Grant Quantatop), the LabEx PALM (Grant number ANR-10-LABX-0039),

the International Balzan Prize Foundation (2013 Prize for Quantum Information Processing and Communication awarded to A. Aspect), the Direction Générale de l'Armement, the french National Research Agency (ANR 15-CE30-0017-04) and the Institut Francilien de Recherche sur les Atomes Froids.

* To whom correspondence should be adressed: david.clement@institutoptique.fr

[1] L. P. Sokol in *Bose-Einstein condensation* (ed. A. Griffin, D. W. Snoke and S. Stringari), p.51, Cambridge University Press (1995).
[2] S. Utsunomiya, L. Tian, G. Roumpos, C. W. Lai, N. Kumada, T. Fujisawa, M. Kuwata-Gonokami, A. Loffler, S. Hofling, A. Forchel and Y. Yamamoto, Nature Physics **4**, 700-704 (2008).
[3] F. Dalfovo, S Giorgini, LP Pitaevskii and S Stringari, Rev. Mod. Phys. **3** 463-512 (1999).
[4] S. W. Hawking, Commun. math. Phys. **43**, 199-220 (1975).
[5] H. P. Yuen, Phys. Rev. A **13**, 2226 (1976).
[6] M. Kohl, T. Stoferle, H. Moritz, C. Schori and T. Esslinger, Applied Physics B 79, 1009 (2004).
[7] K. Xu, Y. Liu, D. Miller, J. Chin, W. Setiawan and W. Ketterle, Physical Review Letters **96**, 180405 (2006).
[8] N. N. Bogoliubov, J. Phys. (USSR) **11**, 23 (1947).
[9] T. D. Lee, K. Huang and C. N. Yang, Phys. Rev. **106** 1135-1145 (1957).
[10] R. J. Donelli, J. A. Donelli and R. N. Hills, J. Low Temp. **44**, 471 (1981).
[11] R. Ozeri, N. Katz, J. Steinhauer and N. Davidson, Rev. Mod. Phys. **77**, 187-205 (2005).
[12] R. Chang, L. Hoendervanger, Q. Bouton, Y. Fang, T. Klafka, K. Audo, A. Aspect, C. I. Westbrook and D. Clément, Phys. Rev. A **90** 063407 (2014).
[13] Q. Bouton, R. Chang, L. Hoendervanger, F. Nogrette, A. Aspect, C. I. Westbrook and D. Clément, Phys. Rev. A **91** 061402(R) (2015).
[14] F. Nogrette, D. Heurteau, R. Chang, Q. Bouton, C. I. Westbrook, R. Sellem and D. Clément, Rev. Scienti. Instrum. **86** 113105 (2015).
[15] M. Schellekens, R. Hoppeler, A. Perrin, J. Viana Gomes, D. Boiron, A. Aspect and C. I. Westbrook, Science **310**, 648-651 (2005).
[16] See supplementary material.
[17] Y. Castin and R. Dum, Phys. Rev. Lett. **77** 5315 (1996).
[18] Y. Kagan, E. L. Surkov, and G. V. Shlyapnikov, Phys. Rev. A **54**, R1753 (1996).
[19] L. Pitaevskii and S. Stringari, Journal of Low Temperature Physics 85, 377-388 (1991).
[20] S. Tan, Ann. Phys. **323**, 2971-2986 (2008).
[21] R. Combescot, F. Alzetto, and X. Leyronas, Phys. Rev. A **79**, 053640 (2009).
[22] We note that T_a may slightly differ from the gas temperature T in the regime $k_B T \simeq \mu$ due to the role of the Hartree-Fock potential induced by the condensate on the thermal component [3].
[23] J. T. Stewart, J. P. Gaebler, T. E. Drake, and D. S. Jin, Phys. Rev. Lett. **104**, 235301 (2010).
[24] C. Luciuk, S. Trotzky, S. Smale, Z. Yu, S. Zhang and J. H. Thwissen, Nature Physics **12**, 530 (2016).
[25] R. J. Wild, P. Makotyn, J. M. Pino, E. A. Cornell and D. S. Jin, Phys. Rev. Lett. **108** 145305 (2012).
[26] P. Makotyn, C. E. Klauss, D. L. Goldberger, E. A. Cornell and D. S. Jin, Nature Physics **10**, 116119 (2014).

SUPPLEMENTARY MATERIAL

Production of gaseous condensates and detection after time-of-flight

Our condensates are produced in the 2^3S_1, $m_J = +1$ internal electronic state. This metastable state has a lifetime of 8000 seconds. To measure the asymptotic momentum distribution $n_\infty(\mathbf{k})$ of the gas, we switch off the optical trap in 2 μs, allowing the cloud to undergo expansion while falling under the influence of gravity. The Micro-Channel Plate (MCP) detector and electronics are described in detail in [14]. The estimated detection efficiency is 25%. The spatial resolution in the plane of the detector is measured to be equal to $\simeq 100$ μm and the time resolution along the vertical axis is 10 μs.

The electronic detector is positioned 55 cm below the trapped gas giving a TOF value of 330 ms. To ensure that the gas expansion is un-perturbed by residual magnetic field gradients present during the TOF, atoms are transferred to the magnetically insensitive $m_J = 0$ state. This transfer is achieved with a radio-frequency (RF) which causes transitions between the magnetic sublevels whose energies have been split by a magnetic bias field with $\Delta E = E_{m_J=+1} - E_{m_J=0} \simeq h \times 10$ MHz. To transfer the atoms independently of their velocity, we use a RF sweep with central frequency 10 MHz and span of $\pm$500 kHz, applied on the atoms after a 2 ms TOF. The RF sweep is 1 ms long at constant RF power. After the RF sweep, we apply a magnetic gradient to push the atoms remaining in the $m_J = \pm 1$ states away from the detector. The RF power, combined with the removal of the $m_J = \pm 1$ states, allows us to control the flux of atoms ($m_J = 0$) striking the detector. We typically operate between 15 and 45% RF transfer efficiency (see **1D density profiles**).

The MCP detector provides a three-dimensional histogram of atom numbers (see Fig. 1(b)). The position of an atom labelled with integer j is given by two-dimensional spatial coordinates (Y_j, Z_j) in the plane of the MCP and the time of arrival t_j. Similarly we note $(Y_0, Z_0, \bar{t} = t_0)$ the coordinates of the center of the cloud whose time of arrival defines the TOF $\bar{t}$ used throughout this work. In the frame centered on the falling could, the position $\mathbf{r}$ of the atom is $\mathbf{r} = (g\bar{t}/2t_j \times (\bar{t}^2 - t_j^2), Y_j - Y_0, Z_j - Z_0)$, accounting for the acceleration g of gravity. The use of the ballistic relation yields the asymptotic momentum distribution $n_\infty(\mathbf{k}) = (\hbar\bar{t}/m)^3\ n(\mathbf{r} = \hbar\mathbf{k}\bar{t}/m, \bar{t})$ (Eq. 1 in the main text). The momentum-space resolution is 0.03 μm^{-1} along directions y and z (in the MCP plane), and 0.01 μm^{-1} along x (orthogonal to the MCP plane). The distributions studied here consist of the the average of roughly 1500 experimental shots. Individual shots have been re-centered to account for slight fluctuations in cloud center-of-mass after the TOF.

1D density profiles

From the three-dimensional asymptotic momentum density $n_\infty(\mathbf{k})$, one-dimensional profiles are generated for the radial and longitudinal cloud directions. Longitudinal profiles are cuts along the z direction (at $k_x \simeq k_y \simeq 0$) with a small integration along the two transverse x and y directions (see below). Radial profiles in the $x - y$ plane are generated from an angular average over azimuthal angles $|\phi| > 45°$, where $\phi = \arctan(k_x/k_y)$ (at $k_z \simeq 0$). This choice of azimuthal angles avoids a defect located on the surface of the micro-channel plate.

Since the experimental signals contain both a high-density condensate and low-density tails with a 4 decade separation in scales, it is necessary to divide the measurement of the density profile into two steps. To measure the condensate momentum components we first use a low RF transfer efficiency (typically 15%). In this low particle flux regime the MCP is far from electronic saturation, but the low-density tails are hard to detect. Secondly to measure the high-momentum tails, we use a high RF transfer efficiency (typically 45%). At high flux of detected particles, the dense condensate locally saturates the MCP, while the low-density wings remain unperturbed. We have verified that the two runs provide identical density profiles at intermediate k where local saturation is not a problem for the high-flux runs and there is sufficient signal in the low-flux runs. The 1D profile for the condensate (low-flux data) has a transverse integration of $\pm$ 0.1 μm^{-1}. The profile for the tails (high-flux data) has transverse integration of $\pm$ 0.8 μm^{-1}. The two-step measurement and transverse integration ensures sufficient signal in the high-momentum tails, while accurately capturing the condensate profile at low-momenta.

In order to illustrate the observed symmetry in region **II** and **III**, we plot measured 1D profiles with a small angular average on ϕ ($\pm 10°$ degrees) along different directions separated by 30°degrees in Fig. 5. The radial 1D profile shown in Fig. 2 (obtained from a large angular average) is reported as a black line in each subplot. The anisotropy of the condensate distribution appears clearly while the momentum profiles in region **II** and **III** have a spherical symmetry.

Mean-field momentum distribution of an interacting gas from time-of-flight

The condensate and its expansion is known to be well modeled by a mean-field interaction [3]. To verify that the observed tails (regions **II** and **III** in Fig. 2(b)) are not an artifact of the condensate, we compare our data to the complete 3D mean-field solution. The mean-field Gross-Pitaevskii (GP) solution beyond the Thomas-Fermi approximation may lead to the appearance of additional momentum components after TOF. These would result

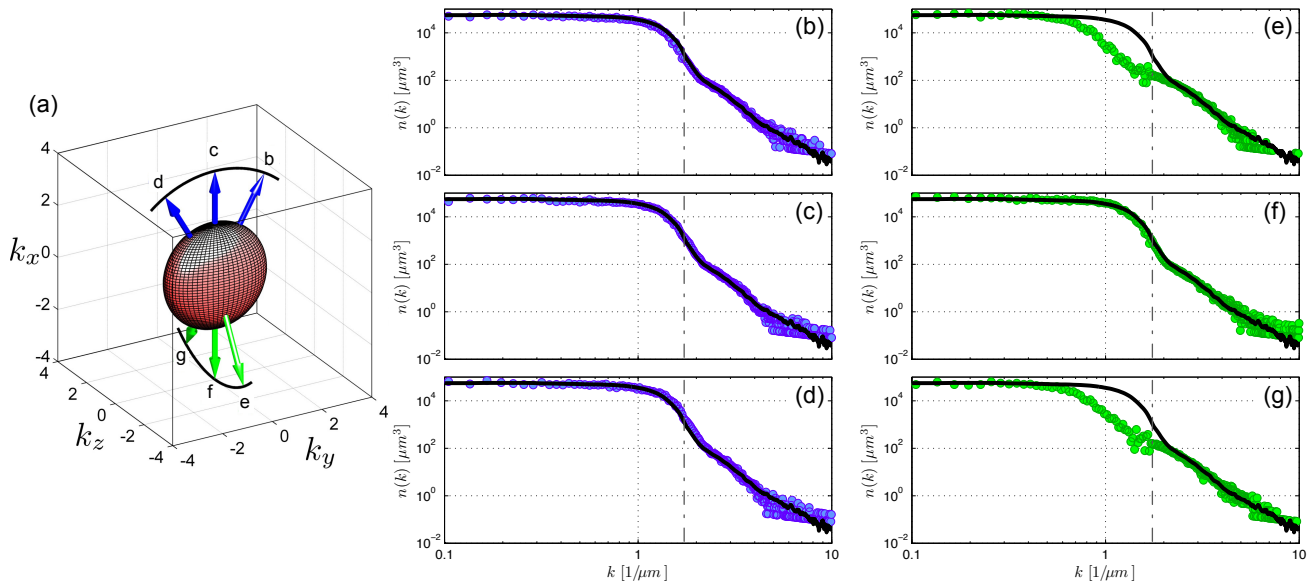

FIG. 5. Observed momentum distributions along various directions, showing the anisotropic condensate distribution and the isotropic components associated with the thermal and the quantum depletion. The vertical dot-dashed line delimits the condensate (low momenta k) and the condensate depletion. **(a)** Sketch of the anisotropic momentum distribution of the condensate in the far-field regime (pancake-shaped distribution). The arrows represent the directions along which we plot the 1D momentum profiles with a small angular average ($\pm 10^\circ$ degrees) in the panels (b)-(g). **(b)-(d)** Blue dots are the measured 1D momentum profiles in the $k_z = 0$ plane. **(e)-(g)** Green dots are the measured 1D momentum profiles in the $k_y = 0$ plane. In each subplot, the solid line is the radial 1D momentum profile plotted in Fig. 2 of the main text (obtained from a large angular average, see above).

from slight modifications of the Thomas-Fermi real-space density occurring on the length scale $(a_{ho}^4/R)^{1/3}$, which fixes the characteristic thickness of the boundary [3] (here a_{ho} and R are, respectively, the oscillator length and the Thomas-Fermi radius and, for simplicity, we have assumed isotropic trapping).

The ground state is obtained by numerical simulation of the Gross-Pitaevskii equation in imaginary time, and the expansion dynamics are performed through real time propagation. The system size used in the calculations limits the simulated TOF. However, the distribution after 2.45 ms is observed to converge, indicating the complete conversion of mean-field interaction energy into kinetic energy. The numerical results for the distribution after a TOF of 2.45 ms are presented in Fig. 6, using the ballistic relation as defined in Eq. 1. The simulations clearly show that the mean-field Gross-Pitaevskii ground state is unable to reproduce the tails observed in the experiment.

Quantum depletion with local density approximation at $T = 0$

In uniform systems Bogoliubov's approach yields a population of momentum state equal to

$$n(k) = |v_k|^2 = \frac{\hbar^2 k^2/2m + mc^2}{2\epsilon(k)} - \frac{1}{2} \tag{4}$$

where $\epsilon(k) = \left[\hbar^2 k^2 c^2 + (\hbar^2 k^2/2m)^2\right]^{1/2}$ is the Bogoliubov excitation spectrum. For a harmonically trapped condensate in the Thomas-Fermi limit, the local speed of sound is $c(\mathbf{r}) = c_0\sqrt{1-(x/R_x)-(y/R_y)^2-(z/R_z)^2}$ with $c_0 = \sqrt{g_s n_0/m}$ the speed of sound at the trap center and $g_s = 4\pi\hbar^2 a_s/m$. In the LDA one finds

$$n(\vec{k}) = \frac{1}{(2\pi)^3}\int |v_{\vec{k}}(\vec{r})|^2 d\vec{r} \tag{5}$$

$$= \frac{R_x R_y R_z}{(2\pi)^2}\left[-\frac{13}{48} - \frac{5k^2\xi^2}{32} + \left(\frac{4+12k^2\xi^2+5k^4\xi^4}{32\sqrt{2}k\xi}\right)\arctan\left(\frac{\sqrt{2}}{k\xi}\right)\right] \tag{6}$$

$$\underset{[k\xi\gg 1]}{\simeq} \frac{R_x R_y R_z}{105\pi^2}\frac{1}{k^4\xi^4} \tag{7}$$

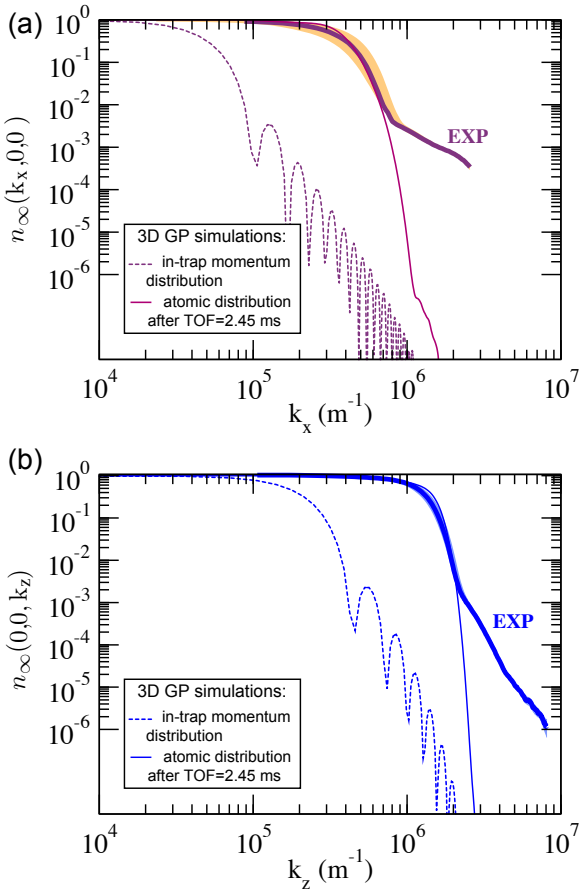

FIG. 6. Simulation of the expansion dynamics of a 3D Bose-Einstein condensate with the mean-field Gross-Pitaevskii equation. The parameters describing the condensate in the numerics (including atom number and trapping frequencies) are those of the experiment. The GP simulation is compared to the experimental data along the longitudinal **(a)** and radial **(b)** direction. It shows an excellent agreement in the region **I** associated with the condensate but does not reproduce the experimental tails. Numerical results and experimental distributions have been normalized to $n_\infty(0,0,0) = 1$.

where $\xi = \hbar/\sqrt{2}mc_0$ is the healing length.

Within the Bogoliubov approach in the LDA approximation, the Tan contact constant, defined as $\mathcal{C} = \lim_{k\to\infty} n(k)k^4$, is equal to $\mathcal{C} = 8/(7\pi)a_s^2 N_0 n_0$, with a_s the s-wave scattering length and N_0 (*resp.* n_0) the condensate atom number (*resp.* the condensate density). For metastable Helium, the calculation gives $\mathcal{C}/N_0 \simeq 2.05 \times 10^{-17} n_0$.

Controlled heating sequence

To increase the temperature of our ultracold gas, we perform a controlled heating sequence using a 3D optical lattice. This sequence involves the adiabatic transfer of the gas from the optical dipole trap to the lattice in 30 ms, followed by a series of non-adiabatic lattice pulses of duration 0.5 ms during which the amplitude of the lattice is set to zero. The gas is then held in the optical lattice for 100 ms during which time it rethermalizes. Finally, we transfer the atom cloud adiabatically back to the initial optical dipole trap in 30 ms. Increasing the lattice depth while keeping the same sequence increases the final temperature of the gas at constant atom number and trapping frequencies.